Applied Optics 46, 4102-4116 (2007)

Investigation into the selection of viewing configurations for three component planar Doppler velocimetry (PDV) measurements

T.O.H. Charrett, D.S. Nobes[1] and R.P. Tatam

Engineering Photonics Group, Centre for Photonics and Optical Engineering, School of Engineering, Cranfield University, Cranfield, Bedfordshire, MK43 0AL, UK

[1] Now at: Department of Mechanical Engineering, University of Alberta, Edmonton, Alberta, T6G 2V4, Canada.

Abstract

A method for the calculation of the three orthogonal velocity components in planar Doppler velocimetry (PDV) using four or more measured velocity components (to the three typically used) is presented. The advantages/disadvantages are assessed using a Monte-Carlo simulation and experimental measurements of the velocity field of a rotating disc. The addition of a fourth velocity component has been shown to lead to reductions in the final errors of up to 25%. The selection of viewing configurations for experiments is discussed by simulating the level of errors in measured velocity components and investigating the final level of errors in the orthogonal velocity components. Experimental measurements of the velocity field of a rotating disc are presented, demonstrating the effect of viewing configuration on the final level of error.

1. Introduction

Planar Doppler velocimetry (PDV)[1,2] also know as Doppler global velocimetry (DGV)[3-6], is a flow measurement technique that can measure three orthogonal velocity components over a plane defined by a laser light sheet. This is accomplished by measuring the Doppler shift of light scattered from particles seeded into the flow and using an absorption line of a molecular gas, usually iodine, as an intensity-to-frequency transducer[5]. The component of the velocity that is measured depends upon the observation direction, $\hat{o}$, and the direction of the illuminating light, $\hat{i}$, and the resulting Doppler shift, $\Delta\nu$, is given by the Doppler formula:

$$\Delta\nu = \frac{\nu(\hat{o} - \hat{i}) \cdot V}{c} \tag{1}$$

where ν is the optical frequency, V is the velocity vector and c is the free space speed of light. The vector difference, $(\hat{o} - \hat{i})$ as shown in figure 1 defines the direction and magnitude the sensitivity vector of a particular view that is a component of the velocity vector at the point of interest.

Measuring the Doppler shift from a single observation direction allows the measurement of a single component of the velocity. By increasing the number of observation directions to at least three, three components of velocity can be measured simultaneously, in a non-orthogonal reference frame. If a 2D detector is used, velocity can be measured over a plane defined by a light sheet. Alternatively, it is possible to measure three velocity components using a single viewing direction and three different illumination directions[7]. It is not possible to measure directly the three orthogonal components of velocity, as there is no practical arrangement of three views, using a single light sheet, where the sensitivity vectors are orthogonal. Therefore,

the three measured velocity components must be transformed from the measurement coordinate system (non-orthogonal) to an orthogonal coordinate system[8]. Previous work has only considered the use of three views, the minimum number required to determine the components of the velocity vector. Inclusion of redundant views has yet to be reported in the literature and in this paper a method of calculating the orthogonal velocity components using more than three measured velocity components is presented and the influence on error is discussed.

The selection of a viewing geometry for a three-component PDV system will affect the level of error in the calculated orthogonal velocity components. There are several considerations that determine the selection of a viewing geometry for use in PDV. These include unobstructed views of the region of interest within a facility, the placement of views with the aim to increase signal and the arrangement of views to minimize error. For many experimental arrangements limited optical access will restrict viewing configurations minimizing the potential for error optimisation. Increased light intensities by placing views in forward scatter would lead to an improved signal-to-noise ratio, however there will be a penalty in additional uncertainty due to determining the angle between the view and illumination vectors[8] and how the measurement uncertainty in the Doppler shift translates to velocity uncertainty.

In our previous publications[9] and those of others[8,10-14] assessments of the level of errors, and their causes, have been investigated. However, these investigations have focussed on determining the level of error in the measured components and there has only been limited investigation[8,15,16] into how these errors propagate through the transformation matrix used to map data from the non-orthogonal to the orthogonal coordinate system. Reinath[8] derived expressions for the uncertainty in the computed orthogonal velocity, Nobes *et al.*[15] suggest the use of the condition number of

the transformation matrix as a measure of the suitability of a viewing configuration and Elliot *et al.*[16] suggest special case geometries where laser frequency fluctuations are cancelled out in the transformation to the orthogonal velocity components. They suggest a method of optimising a three-component PDV system using these special case geometries and minimising the condition number. However, due to viewing constraints in an experiment it may not be possible to select this special case viewing geometry.

This paper will investigate the optimisation of the viewing geometry for a three-component PDV system. In section 3 the factors influencing the selection of viewing geometry are described. In order to assess the performance of different viewing configurations a number of methods are described in section 4. The use of the condition number of the transformation matrix is discussed in section 4.1. A Monte-Carlo simulation of the processing of PDV data with known quantities of noise introduced is described in section 4.2 and an experimental arrangement of a two-frequency PDV system, used to make measurements on a rotating disc, is described in section 4.3. These are then used to investigate the factors affecting the relative performance of several viewing configurations in section 5, and to investigate the benefits of using additional velocity components in the calculation of the orthogonal velocity components in section 6. Finally, in section 7, experimental data is presented that is compared to the simulation results demonstrating the use of additional velocity components.

2. Methods for the computation of the orthogonal velocity components

Throughout previous work in PDV, researchers have concentrated upon either making single velocity component measurements[14] or three-component velocity measurements[17-19] using three

measured non-orthogonal components. To determine the three orthogonal velocity components at a location in the flow it is necessary to measure at least three non-orthogonal velocity components, which can then be mapped to an orthogonal coordinate system aligned with the experiment. Using the definitions shown in figure 2 the velocity components can be converted to the orthogonal velocity components, U, V and W using the following expressions given by Reinath[8]:

$$U = \frac{1}{\det([a])}\left[|U_1|(Y_2Z_3 - Y_3Z_2) - |U_2|(Y_1Z_3 - Y_3Z_1) + |U_3|(Y_1Z_2 - Y_2Z_1)\right] \quad (2)$$

$$V = \frac{1}{\det([a])}\left[-|U_1|(X_2Z_3 - X_3Z_2) + |U_2|(X_1Z_3 - X_3Z_1) - |U_3|(X_1Z_2 - X_2Z_1)\right] \quad (3)$$

$$W = \frac{1}{\det([a])}\left[|U_1|(X_2Y_3 - X_3Y_2) - |U_2|(X_1Y_3 - X_3Y_1) + |U_3|(X_1Y_2 - X_2Y_1)\right] \quad (4)$$

Where:

$\|U\|_1$	Magnitude of the measured component from camera view 1
$\|U\|_2$	Magnitude of the measured component from camera view 2
$\|U\|_3$	Magnitude of the measured component from camera view 3
X_1,Y_1,Z_1	Unit vector components defining the direction of ($\hat{o}_1$ - $\hat{i}$)
X_2,Y_2,Z_2	Unit vector components defining the direction of ($\hat{o}_2 - \hat{i}$)
X_3,Y_3,Z_3	Unit vector components defining the direction of ($\hat{o}_3 - \hat{i}$)
U,V,W	Orthogonal velocity components, horizontal, vertical and out-of-plane respectively.

det([a]) $$\det([A]) = X_1Y_2Z_3 + Y_1Z_2X_3 + Z_1X_2Y_3 - Z_1Y_2X_3 - X_1Z_2Y_3 - Y_1X_2Z_3$$

If more than three different observations are taken, a new system of equations is required to transform the data. A system of equations for an over-redundant set of measurements can be solved using a least squares method. Restricting the number of measurements for this development to four to match the experimental system used here, a system of equations to be solved can be expressed as:

$$\begin{bmatrix} |U_1| \\ |U_2| \\ |U_3| \\ |U_4| \end{bmatrix} = \begin{bmatrix} X_1 & Y_1 & Z_1 \\ X_2 & Y_2 & Z_2 \\ X_3 & Y_3 & Z_3 \\ X_4 & Y_4 & Z_4 \end{bmatrix} \begin{bmatrix} U \\ V \\ W \end{bmatrix} \tag{5}$$

This is equivalent to:

$$U_m = J\vec{V} \tag{6}$$

Where $\vec{V} = (U,V,W)$, U_m is the column vector containing the measured velocity magnitudes and J is the transformation matrix. The general least squares method for linear equations[20] is given by:

$$\vec{V} = (J^T wJ)^{-1} J^T wU_m \tag{7}$$

Here w is the weighting matrix, and has the form;

$$w = \begin{bmatrix} w_1 & 0 & 0 & 0 \\ 0 & w_2 & 0 & 0 \\ 0 & 0 & w_3 & 0 \\ 0 & 0 & 0 & w_4 \end{bmatrix} \tag{8}$$

The matrix allows each equation to be ranked, with larger values indicating greater importance and $w_{1\text{-}4}$ are the relative weightings.

This produces a result that attempts to minimise the difference between each of the four measured values and the calculated values resulting in a 'best fit' value for *U*, *V* and *W* although this may not be the true value. Therefore (5) and (6) can be written:

$$\begin{bmatrix} |U_1| \\ |U_2| \\ |U_3| \\ |U_4| \end{bmatrix} \approx \begin{bmatrix} X_1 & Y_1 & Z_1 \\ X_2 & Y_2 & Z_2 \\ X_3 & Y_3 & Z_3 \\ X_4 & Y_4 & Z_4 \end{bmatrix} \begin{bmatrix} U \\ V \\ W \end{bmatrix} \tag{9}$$

$$U_m \approx J\vec{V} \tag{10}$$

Solving (10) for $\vec{V}$ gives:

$$\begin{bmatrix} U \\ V \\ W \end{bmatrix} = L \begin{bmatrix} (df - ee)g + (ce - bf)h + (be - cd)j \\ (ce - bf)g + (af - cc)h + (bc - ae)j \\ (be - cd)g + (bc - ae)h + (ad - bb)j \end{bmatrix} \tag{11}$$

Where:

$$a = \sum_i X_i^2 w_i \qquad b = \sum_i X_i Y_i w_i \qquad c = \sum_i X_i Z_i w_i$$
$$d = \sum_i Y_i^2 w_i \qquad e = \sum_i Y_i Z_i w_i \qquad f = \sum_i Z_i^2 w_i$$

$$g = \sum_i X_i U_i w_i \qquad h = \sum_i Y_i U_i w_i \qquad j = \sum_i Z_i U_i w_i$$

$$L = \frac{1}{a(df - ee) - b(bf - ce) + c(be - dc)}$$

Although the above analysis has used only four velocity components, the solution given in equation (11) is general and can be expanded to more than four components where *i* is the number of velocity components to be mapped. This method will be described as the 4C method in the remainder of this paper and the method given by equations (2), (3) and (4) as the 3C method, referring to the number of velocity components used in the transformation.

3. Factors influencing the selection of a viewing geometry

The level of uncertainty in the final computed orthogonal velocity components will depend both on the level of uncertainty in each measured component to be transformed, and on the transformation process itself. The effect of a particular observation direction on the uncertainty of an individual measured velocity component can be investigated by considering the individual sources of uncertainty. There are three factors to be considered, firstly uncertainty in determining the sensitivity vector from the observation and laser illumination directions will result in variable uncertainty in the velocity component depending upon observation direction. The second is due to how the uncertainty in the measured Doppler shift will convert to a measured velocity component uncertainty. The third factor is the variation in signal levels due to the Mie scattering intensities. Views located in forward scatter will have a higher signal level than those in back scatter, resulting in less uncertainty in determining the Doppler frequency shift and hence less uncertainty in the measured velocity component.

3.1. *Velocity uncertainty due to determining the sensitivity vector*

Elliott and Beutner[14] give a derivation for the level of error in determining the sensitivity vector ($\hat{o}$- $\hat{\imath}$) by considering the error in the angle between the two vectors from the Doppler equation using:

$$\Delta U_n = \frac{\partial U_n}{\partial \phi}\Delta\phi = \frac{-U_n}{2\tan(\phi/2)}\Delta\phi \tag{12}$$

Where ϕ is the angle between $\hat{o}$ and $\hat{\imath}$, $\Delta\phi$ is the error in this angle, and U_n is the velocity component. The level of error as a function of the view direction can be represented graphically by considering $\hat{o}$ and $\hat{\imath}$ in a spherical coordinate system from which ϕ can be determined. figure 3 shows this variation of the uncertainty in the measured velocity component, as the observation direction is varied. Here the colour represents the level of uncertainty in the measured velocity component for the observation direction represented by the position on the surface. Values were calculated using equation (12) and an uncertainty in ϕ of 1^o. The observation direction was varied between $\pm 60^o$ from the normal to the light sheet, which is propagating in the positive X direction in the XY plane. As the magnitude of the uncertainty is also dependant upon the velocity magnitude the calculations for two different velocities, (50,50,10) m/s and (30,300,30) m/s, are shown. It can be seen from equation (12), and the pictorial representation in figure 3, that as the observation vector moves into forward scatter, ϕ approaches 0^o signifying that $\hat{o}$ and $\hat{\imath}$ are approaching a parallel direction and the level of error increases.

The error in this angle, ϕ, arises directly from the determination of the vectors $\hat{o}$ and $\hat{\imath}$. Determination of $\hat{o}$ can be physically measured as a bulk direction from the region-of-interest in the flow to the detectors. However, the observation direction will vary for each pixel across the

image introducing a systematic error. Alternatively, calibration images of a target can by used to calculate the observation vectors for each pixel in the image from images of a known target[21]. Some measurement uncertainty may also be introduced due to misalignment of the target with the light sheet. The uncertainty in the laser illumination direction, $\hat{\imath}$ has three sources; the first is a measurement uncertainty in the bulk illumination direction; the second is due to a variation in illumination direction due to the divergence of the laser sheet in the measurement plane; and the third is convergence/divergence of the laser sheet thickness. It is possible to correct to a certain extent for the last two of these effects when processing the PDV data; however there will still be a degree of uncertainty in the laser illumination direction.

As well as introducing a variation in the error on the measured velocity components the uncertainty in the view angles will also introduce error into the transformation from the measured velocity components to the orthogonal velocity components. Reinath[8] gives expressions for the uncertainty in the orthogonal transformation for the 3C method. Similar expressions can be found for the 4C method with the added contributions from the fourth measured velocity component and the fourth sensitivity vector and these are shown in equations (13)-(15). From these equations it can be seen that the level of this uncertainty is related to the magnitude of the velocity components and will therefore also vary with flow velocity.

$$\Delta^2 U = \sum_n \left[\left(\frac{\partial U}{\partial |U_n|} \Delta |U_n| \right)^2 \right] + \sum_n \left[\left(\frac{\partial U}{\partial X_n} \Delta X_n \right)^2 \right] + \sum_n \left[\left(\frac{\partial U}{\partial Y_n} \Delta Y_n \right)^2 \right] + \sum_n \left[\left(\frac{\partial U}{\partial Z_n} \Delta Z_n \right)^2 \right] \quad (13)$$

$$\Delta^2 V = \sum_n \left[\left(\frac{\partial V}{\partial |U_n|} \Delta |U_n| \right)^2 \right] + \sum_n \left[\left(\frac{\partial V}{\partial X_n} \Delta X_n \right)^2 \right] + \sum_n \left[\left(\frac{\partial V}{\partial Y_n} \Delta Y_n \right)^2 \right] + \sum_n \left[\left(\frac{\partial V}{\partial Z_n} \Delta Z_n \right)^2 \right] \quad (14)$$

$$\Delta^2 W = \sum_n \left[\left(\frac{\partial W}{\partial |U_n|} \Delta |U_n| \right)^2 \right] + \sum_n \left[\left(\frac{\partial W}{\partial X_n} \Delta X_n \right)^2 \right] + \sum_n \left[\left(\frac{\partial W}{\partial Y_n} \Delta Y_n \right)^2 \right] + \sum_n \left[\left(\frac{\partial W}{\partial Z_n} \Delta Z_n \right)^2 \right] \quad (15)$$

3.2. Velocity uncertainty due to the error in the measured Doppler shift

The second factor, error in the measured velocity component due to uncertainty in the Doppler shift, can be investigated by considering the following error equation derived from the Doppler equation:

$$\Delta U_n = \frac{\partial U_n}{\partial(\Delta\nu)} \Delta(\Delta\nu) = \frac{\lambda}{\sin(\phi/2)} \Delta(\Delta\nu) \quad (16)$$

Where $\Delta\nu$ is the Doppler shift, $\Delta(\Delta\nu)$ is the uncertainty in the Doppler shift, λ is the wavelength of the illuminating light, ϕ is the angle between the observation and illumination vectors and U_n is the magnitude of the measured velocity component. Contributions to the error in determining the Doppler shift will come from camera noise, the error in measuring or modelling the iodine transmission line used and uncertainty in the laser frequency. The magnitude of the uncertainty in Doppler shift will be constant for all viewing directions, however the resulting uncertainty in the velocity component will not be constant and will be dependant upon viewing direction. The variation in the measured velocity component uncertainty for a 5MHz Doppler shift uncertainty is shown in figure 4. The plot again shows that as the view moves further into forward scattering there will be an increase in the velocity component uncertainty.

3.3. Mie scattering intensity

The third factor to consider is the Mie scattering intensities, as although backscatter angles reduce the level of uncertainty due to the above effects, the scattering intensities at these angles

will be greatly reduced resulting in higher measurement uncertainty. The plot shown in figure 5 shows the relative intensities of the Mie scattering for different view angles.

4. Evaluation methods for assessing PDV viewing geometries

The effect that the choice of viewing geometry has on the final level of uncertainty in the computed orthogonal velocity components, will be important in design considerations for new experiments and the evaluation of established facilities to determine if PDV is applicable. In order to investigate this, several viewing configurations typical of those found in the literature were defined and are shown in schematic form in figure 6. A spherical coordinate system can be used to describe each view using two angles; α the rotation around from the X-axis is the XZ plane and β, the elevation from the XZ plane. The Cartesian components and view angles are given in table 1. The configurations chosen are all practical for experimental implementations, including two that have been previously reported[7,8]. For each configuration, except configuration E which uses multiple light sheets, the illumination vector (laser sheet) is in the positive X direction. To investigate the benefits of using additional data to calculate the orthogonal velocity components a fourth view was added to each of the configurations. Where possible this view was selected to have similar viewing angles to the other three, although for the reported configurations no account was taken for possible obstruction of this additional view.

For configuration A, the four views are aligned so that each of the view vectors, from the origin of the coordinate system to the cameras, are aligned such that the bulk view vector of each view is a function of only two of the Cartesian co-ordinate system variables. The views are all on the negative Z-axis side of the laser sheet. Configuration B again has all four views on the same side of the light sheet. This configuration is similar to configuration A however the set-up aims to

increase the angle between the sensitivity vectors. The reported sensitivity vectors of Reinath[8] are used in configuration C. This is similar to Configuration B except that one view has been rotated, by 180°, about the Y-axis placing it on the opposite side of the laser sheet. The fourth view has been added between views 1 & 2, level with view 3. All four views are located in forward scatter with respect to the laser direction vector. Configuration D uses similar view angles to configuration C expect that now the first three views are all located in back scatter. Configuration E follows the configuration of Roehle *et al.*[7], which consisted of a single view and three laser sheets in the same plane from different orthogonal directions. The fourth measured component is added by including a fourth illumination direction. The sensitivity vectors all have a positive Z-axis component and at the origin are a function of only two of the Cartesian co-ordinate variables. Configuration F uses a similar multiple light sheet approach with two observation directions and two laser sheets.

4.1. The condition number of the transformation matrix

How well the measured velocity components can be mapped to the orthogonal Cartesian co-ordinate system can be described empirically by the value of the condition number of the transformation matrix. The condition number, $\kappa(A)$, of a matrix can be used as a measure of the sensitivity of the solution of the system of linear equations defined by the matrix to errors in the data and is defined as[22]:

$$\kappa(A) = \|A\| \|A^{-1}\| \tag{17}$$

Here, A, is the transformation matrix and $\|A\|$ is the norm of the matrix and can be defined in several different forms. In this paper four definitions of the condition number are used based on four different definitions of the norm of the matrix.

κ_1 The norm is based on the largest column sum in *A*

κ_2 The norm is based on the largest column value in *A*

κ_3 The norm is based on Frobenius-norm of matrix *A*, $\sqrt{\sum diag(A'.A)}$

κ_4 The norm is based on the largest row sum in *A*.

The computed condition number for the ideal case, where the three sensitivity vectors are aligned with the axes of a Cartesian co-ordinate system is shown in table 2. The closer the value of κ(A) to this ideal case the better conditioned the matrix is for transforming measured results to the orthogonal coordinate system.

Values for the different condition numbers were calculated using the built-in Matlab programming language function, for the first three views for each of the viewing configurations defined in table 1. These are presented in table 3, here only three views for each configuration are considered. Low values of κ(A) are achieved for configurations where the sensitivity vectors are well spread. This is evident for configurations where one of the sensitivity vectors is on the opposite side of the light sheet (Configurations C & D) compared to the having all three sensitivity vectors on the same side (Configurations A & B). There is a small change in the view direction vectors in Configuration A to Configuration B. This however leads to a halving of κ(A). A further reduction can be achieved on the value of Configuration B by moving one of the view directions to the other side of the light sheet as in Configuration C.

For all definitions of κ(A) the magnitude of κ(A) shows a similar trend. Low values of κ(A) are obtained for conditions where the sensitivity vectors are well spread or are close to orthogonal

and are close to the directions of the Cartesian co-ordinate system of the experiment. High values of $\kappa(A)$ are determined where the sensitivity vectors are similar.

4.2. Monte-Carlo simulation of error sources in a PDV system

To analyse and investigate error sources in PDV, a Monte-Carlo simulation has been developed to model conditions typically found in PDV experiments and are summarised in table 4. The process used in the model is shown in figure 7, initially a viewing configuration is defined and the sensitivity vectors for each view calculated. This is done using a simple pin-hole model of the collection optics to calculate the views angles for each pixel across the image. This includes the variation in observation direction across the image as would be found in experiments. From these the sensitivity vector for each pixel can be found by subtracting the defined laser illumination vector. The rays within the light sheet were assumed to be parallel, not diverging as would be found in some experiments. Using the Doppler equation and the calculated sensitivity vectors, images representative of the Doppler shift in the frequency of scattered light were generated for a defined velocity field, (U,V,W) m/s. One such image was generated for each of the four different views allowing the assessment of both three and four component PDV systems. An experimental measurement of the iodine absorption line was then used to convert from Doppler shift to filtered transmission images. The relative Mie scattering intensity for each of the views was then calculated using a distribution of particle sizes. The transmission images are then converted to intensity images (equivalent to the filtered signal and unfiltered reference images captured in a PDV experiment). These images are scaled to account for the Mie scattering intensities where it is assumed that the full camera range can be used at a scattering angle of 90^{o}, as the signal levels of views in forward scatter can be attenuated to avoid saturation of the CCD. Views with scattering intensity equal or greater than this are assumed to have a maximum

intensity (at 100% transmission) of 4000 counts. Views with lower scattering intensities are scaled accordingly.

From these computed Doppler shift images the non-orthogonal velocity components can be calculated as in standard PDV processing. Subsequent transformation back to orthogonal velocity components recovers the original velocity field perfectly. The only error introduced is the rounding errors in the calculations and the uncertainty in the measured iodine absorption line used. Other errors sources can be investigated by adding a known amount of noise at different stages simulating what is found in a typical experiment. Three possible ways of adding noise were implemented. Firstly the contribution from the CCD camera noise, ERR_{CCD} can be introduced. This is added to the calculated intensity images by converting this intensity in counts to photoelectrons detected at each pixel found using the analogue-to-digital conversion factor for the CCD camera. Noise is then modelled using a Poisson distribution and rounding the result of the conversion back to counts introduces the effect of analogue-to-digital truncation. The second method is adding uncertainty to the Doppler shifts, $ERR_{Dop.}$ This is modelled by adding a random quantity of noise to each pixel in the Doppler shift image from a normal distribution. This is used to model sources of error such as the laser frequency uncertainty and iodine transmission uncertainty. The third source of error added, ERR_{View}, is used to model the error introduced by uncertainty in the measurement of the viewing angles. To include ERR_{View} a random quantity of noise, taken from a normal distribution, is added to each pixel of the view angle images. New sensitivity vectors, that include this error, are then calculated. When both ERR_{CCD}, ERR_{Dop} and ERR_{View} are included in the calculation of the velocity component, this will be described as having had variable error added, ERR_{Var}, referring to the fact that the level of error in the

calculated velocity components will depend upon the observation direction[8] due to the Mie scattering and the Doppler formula. For the purpose of this discussion a fourth method for adding noise was used. Here a random quantity of noise is added to each pixel after the calculation of the velocity component; this will be termed as constant error, ERR_{Con} as the same level is added regardless of observation direction. This has no physical significance and is only used in the assessment of the transformation to orthogonal velocity components discussed later. Once all of the measured velocity components have been generated they are then transformed to the orthogonal velocity components. The level of propagated error is then found by comparison of the calculated orthogonal velocity components with the reference velocity field that was defined initially.

4.3. PDV experimental configuration

The error sources assessed theoretically in previous sections were investigated experimentally (results presented in sections 5 and 7) using the two-frequency PDV (2ν-PDV) system developed by Charrett *et al*.[18,23] is shown in figure 8. This system uses fibre-imaging bundles[17] to port up to four views of the region of interest to a single CCD camera (LaVision - SensiCam 12bit, 1280x1064 pixels) which views the combined end of the fibre imaging bundle through an iodine absorption cell. The light sheet was generated with an argon ion laser (Spectral Physics BeamLok 2060) that is run single line (514.5nm) using a temperature-tuned etalon. The light sheet was formed using a beam scanning technique described by Roehle *et al*.[7]. The signal image is collected with the laser tuned to the 50% transmission of an iodine absorption line. A reference image is collected with the laser tuned to a second frequency that is on a portion of the iodine spectrum for which there is full transmission through the filter.

The 2ν-PDV system was used to measure the well-defined velocity field of a rotating disk. Four views of the disk where captured and pixel view vector and position scaling information was determined using images of a target by the method of Nobes *et al.*[21]. The measurement error of the final orthogonal velocity components was then determined by subtracting the velocity field determined from the rotational frequency of the disk from the PDV measurements. The advantage of using this PDV configuration is that it does not include additional uncertainties due to the polarisation sensitivity of the beam splitter and pixel matching effects of using two CCD cameras to simultaneously collect signal and reference images. There are however disadvantages associated with the technique including variation in the scattered light intensity between images due to seeding concentration changes and the constancy of the illumination intensity although this will not be a problem when making measurements using a rotating disc.

5. Investigation of PDV error sources and their influence on measurement uncertainties

The impact of view angle on velocity component uncertainty was investigated experimentally using the 2ν-PDV system described in section 4. Four different components, of the velocity field of a rotating disc, were measured with each of the four bundle arms positioned at angles located increasingly into forward scatter, so that the values of ϕ were 90^o, 70^o, 50^o and 30^o respectively. Images of a calibration target were used to de-warp the views onto a scaled image and to calculate the observation directions for each view[21]. This was then used to calculate theoretical velocity components, based upon the calculated position scaling, observation direction information and the frequency of rotation of the disc. These theoretical velocity components

were then subtracted from the experimental measured velocity components, and a histogram taken of the remaining values, giving a measure of the level of error in each component.

The results, figure 9, show that the magnitude of the error increases as the view moves into forward scatter as ϕ tends to zero. The error approximately doubles between when the view is normal to the light sheet and when located predominantly in forward scatter. This result suggests that while higher signal intensity levels are attainable in forward scatter there is a penalty in the uncertainty of the measured component. However, it should be noted that these measurements where made on a rotating disc where the scattering intensity varies less with view angle than it would for a seeded flow.

The Monte-Carlo simulation was then used to assess each of the viewing configurations defined in section 4. The effect of calculating the uncertainty in each measured velocity component from the observation direction was compared to the situation where all of the measured velocity components are assumed to have the same uncertainty. The variable error (ERR_{Var}) was simulated by calculating ERR_{CCD} from the Mie scattering intensity, adding a Doppler shift uncertainty (ERR_{Dop}) of 2.5MHz and an uncertainty in each of the view angles (ERR_{View}) of 0.1^{o}. For the simulation using a constant level of uncertainty in the velocity components (ERR_{Con}) the noise added to each component had a standard deviation of 2.0m/s. This value was chosen to produce final uncertainties of typical experimental magnitude.

The level of propagated noise in the orthogonal velocity components was found by considering the orthogonal component residuals, which are the calculated velocity fields minus the known velocity fields. Figure 10 shows histograms of this remaining noise, for two configurations (A

and B) for each of the orthogonal components U, V and W using the 3C method. A velocity of (10,100,10) m/s in the U, V and W components respectively was used. The standard deviation of the normal distribution can be used as a measure of the level of error for each result. These are shown for the different viewing configurations using the first three components, in table 5.

Figure 10 and table 5 demonstrate that if a constant level of noise is added to each measured velocity component then configuration B will lead to smaller final errors than configuration A in all three orthogonal components. This is because configuration B has better conditioning for the transformation (condition number ~ 7) compared to configuration A (condition number ~14). However, when variable uncertainty is included the conditioning of the matrix becomes less important, such that the advantage of configuration B is reduced. This is due to configuration B having two views (views 1 & 2) significantly into forward scatter leading to larger uncertainties in these measured velocity components although the better conditioning still leads to lower uncertainties in the U and W components. Configuration A also has view 3 located in backscatter leading to lower signal levels and increased uncertainty in this component. If the components are measured with separate integration times to ensure high signal levels then the uncertainty in this component could be reduced although background scattering may become more of an issue if the camera integration times are high. The measured velocity component uncertainty is related to the flow velocity therefore if a different velocity field is used the results will change. Simulations for a velocity field of (30,300,30)m/s are shown in table 5 for configurations A and B. For this higher velocity field the advantage of configuration B is again reduced indicating that a prior knowledge of the magnitudes of the flow velocities will be helpful in selecting the view configuration to be used.

The results for all of the configurations are also presented in table 5. Configuration C is better that either A or B due to a combination of better conditioning and good signal levels. Experimentally this is a good configuration as the views are located in forward scatter, leading to good scattering levels and reduced integration times minimizing the effect of background light. Configuration D is better still due to good conditioning and the location of views in backscatter resulting in smaller uncertainties in these measured components as described in section 3. However, the location of the views in backscatter may lead to problems with long integration times and background light. The multiple light sheet approach modelled in configuration E provides good transformation to the orthogonal components, and reasonable scattered light levels, with all of the measured components having similar signal levels. Additionally the use of a single camera will overcome image misalignment errors between the views, which have not been included in this model. A disadvantage however is that the components are no longer captured simultaneously so only time averaged flows can be measured. Configuration F uses two views and two light sheets and again it was assumed that each of the components is captured sequentially so that all views will have similar signal levels. The conditioning for this transformation is not as good as for configuration E hence the uncertainties are greater.

The simulation confirms that generally for a lower condition number the residual error will be lower. However, the effect of Mie scattering intensity and Doppler formula uncertainty, discussed in section 3, will play an important role in the selection of a viewing configuration. The effect of the magnitude of the velocity field can also influence view selection and prior knowledge of the flow would be helpful in selecting the view configuration.

6. Simulation of transformation to orthogonal velocity components using additional measured velocity components.

In order to assess the benefits of the 4C method of calculating the orthogonal velocity components, the computed velocity components were processed using the first three components (with the 3C method) and all four components (using the 4C method). The residuals were then calculated as before. Figure 11 shows the histograms of the residuals for both configuration A and configuration B for both methods of calculating the orthogonal components. The standard deviations for the other configurations are shown in table 6 for calculations using the 3C method and the 4C method. Variable uncertainty was introduced to each component depending upon the observation direction as described in section 5 and all the components were equally weighted in the calculation using the 4C method.

Figure 11 shows that the addition of a fourth measured component significantly lowers the level of error in two (U and W) of the three orthogonal components while the third (V) remains unchanged. For these configurations no attempt was made to optimise the positioning of the fourth view, rather it was placed so that the viewing angles were similar to the original three views. Similar improvements can be seen for the other configurations in table 6 with one or two components having improved error levels with the remaining components unchanged or slightly degraded.

The actual benefit of calculating the orthogonal velocity components using additional components will depend upon the flow to be measured as well as optical access constraints. The use of extra information from redundant views appears to be of greater benefit for poorly conditioned viewing configurations such as configurations A and B and so could be of benefit where optical access prevents an ideal viewing configuration using three views. However it may be that by selecting the 'best' three of the four views the reduction achieved using the 4C method can be obtained using the conventional 3C method. This was investigated by calculating the U, V and W components using all four combinations of three views and the 3C method. The lowest achievable error level in each orthogonal component using the 3C method was found. This is shown in table 7 along with the error levels found using the 4C method and the percentage change in standard deviation when changing from using the 'best' 3C method to the 4C method.

When the best three views are used to calculate each orthogonal velocity component, the benefit of calculating the orthogonal velocity components using the 4C method is reduced. Use of the 4C method however provides a further improvement the uncertainty of out-of-plane component for all of the configurations and some improvement in the other components for several of the configurations. From this it can be seen that the benefit of measuring a fourth velocity component will depend upon the viewing configuration. The greatest benefit is for poorly conditioned configurations were adding a fourth component could significantly improve the final uncertainty. Optimal results will be achieved by using a combination of the two methods, selecting the optimal method for the calculation of each orthogonal component. For example if configuration C were used, the results of the model would suggest that the U and W components

should be calculated using the 4C method whilst the V component should be calculated using the 3C method using the best three of the four views.

7. Experimental investigation of error propagation using a two-frequency PDV (2ν-PDV) system

The Monte-Carlo simulation discussed in the previous sections can be used as a tool to determine the most significant source of error by comparison with an experiment. The simulation was configured to model the conditions of an experiment where a 2ν-PDV system measured the velocity field of a rotating disc[18]. The disc rotated at a frequency of 105Hz and the common field of view after de-warping was approximately 100x100mm, giving a velocity range of ±33m/s in the field of view. The effect of low-pass filtering has not been investigated here, and all results, both modelled and experimental are presented without any filtering being applied. It should be noted that all of this analysis is non-specific to 2ν-PDV and is equally applicable to a conventional PDV system.

Two configurations similar to A and B, previously described, where used, with the views positioned as close as possible to those defined. However due to experimental limitations less elevation than desired was possible. The experimental view angles are shown in table 8, where the values differ from those defined in table 1 for configurations A and B. The desired values are shown in parenthesis.

The influence of different view configurations is shown in figure 12 where the simulation was adjusted to give results of error that compare well with the experimental results. The Mie scattering calculation for small-dispersed spherical particles in air in the model was not used as

the variation of scattering intensity for a solid surface will be different. Instead the uncertainty in the Doppler shift (ERR_{Dop}) was assumed to be ~5 to 5.5MHz depending upon the received scattered light intensity. The viewing directions were calculated using the results of the de-warping process[21]. It is known that this technique does not work as well for views that are close to perpendicular to the light sheet, the uncertainty in the viewing angles (ERR_{View}) used was therefore between 0.1^o and 0.8^o depending upon the viewing angles for each view. The comparison shows that the simulation correctly predicts the effect of changing view configuration.

The effect of using additional velocity components is shown in figure 13. Here orthogonal components calculated using the 3C method are compared to those calculated using the 4C method, for configurations A. Details of the standard deviation of the error are shown in table 9 for both configurations and both methods. As predicted earlier by the Monte-Carlo simulation, the addition of a fourth measured velocity component improves the error level in at least two of the final orthogonal components. This is apparent for both view configurations used. For configuration A the error of the U and W components respectively are reduced by ~15% and ~25% when using a fourth velocity component. The reductions for configuration B are less but the U component error is still reduced by ~9% when using a fourth component while the W component is reduced by ~25%. The results show that as predicted by the simulation, the additional information of even a single extra measurement can reduce the level of error.

8. Conclusions

A Monte-Carlo simulation was developed to assess the error sources, the influence of viewing geometry and the benefits of additional data for PDV systems. The simulation was compared to experimental results made using a 2ν-PDV system and used to identify the error levels of different sources. The simulation showed that the performance of a three-dimensional PDV system is strongly influenced by the geometry of the experimental configuration, including the direction of the laser sheet and the choice of viewing angles. Even though the error level of individual measured velocity components may be acceptable, the transformation matrix that is used to map the results to an orthogonal co-ordinate system can significantly amplify this noise. The condition number of the transformation matrix can be used as a rough guide to assess the impact the transformation will have on results. Although conditioning alone is not the only factor that should be taken into account when selecting a viewing configuration with scattered light intensity and viewing angle both affecting the level of uncertainty in the non-orthogonal components.

As both the error level of individual velocity components and the error propagated by the transformation to orthogonal components are dependant upon the flow velocity. This result indicates that a prior knowledge of the expected velocities will be useful in determining a suitable viewing configuration.

The addition of a fourth measured velocity component has been shown to significantly reduce the level of errors in the orthogonal components. This result was most significant for view

conditions where the transformation matrix was poorly conditioned. The measurement of four velocity components is simple to implement when working with a PDV system using imaging fibre bundles. It is may also be possible to further improve the level of errors in some of the orthogonal velocity components by weighting (in the 4C method) the components depending upon their expected level of error however this requires further investigation.

9. Acknowledgements

This work was funded by the Engineering and Physical Sciences Research Council (EPSRC), UK.

10. References

1 H.D. Ford and R.P. Tatam, "Development of Extended Field Doppler Velocimetry for Turbomachinery Applications", *Optics and Lasers in Engineering*, **27**, 675-696, (1997).

2 M. Samimy and M.P. Wernet, "Review of Planar Multiple-Component Velocimetry in High-Speed Flows", *AIAA Journal*, **38**, 553-574, (2000).

3 H. Komine, "System for measuring velocity field of fluid flow utilizing a laser-Doppler spectral image converter", United States Patent , Number 4,919,536, (1990).

4 J.F. Meyers and H. Komine, "Doppler Global Velocimetry: a new way to look at velocity", *Laser Anemometry*, **1**, 273-277, (1991).

5 H. Komine, S. Brosnan, A. Litton, and E. Staepperts," Real-Time Doppler Global Velocimetry", *AIAA 29th Aerospace Sciences Meeting*, (Reno, Nevada, 1991), Paper 91-0337.

6 J.F. Meyers, "Development of Doppler Global Velocimetry as a Flow Diagnostics Tool", *Measurement Science and Technology*, **6**, 769-783, (1995).

7 I. Roehle, C. Willert, R. Schodl, and P. Voigt, "Recent Developments and Applications of Quantitative Laser Light Sheet Measuring Techniques in Turbo machinery Components", *Measurement Science and Technology*, **11**, 1023-1035, (2000).

8 M.S. Reinath, "Doppler Global Velocimeter Development for the Large Wind Tunnels at Ames Research Center", NASA , Technical Memorandum 112210, (1997).

9 H.D. Ford and R.P. Tatam," Imaging System Considerations in Doppler Global Velocimetry", *Proc. SPIE*, (San Diego, CA, 1995), 2546, 454-464.

10 G.L. Morrision and C.A. Gaharan, "Uncertainty estimates in DGV Systems due to pixel location and velocity gradients", *Measurement Science and Technology*, **12**, 369-377, (2001).

11 J.F. Meyers, J.W. Lee, and R.J. Schwartz, "Characterization of Measurement Error Sources in Doppler Global Velocimetry", *Measurement Science and Technology*, **12**, 357-368, (2001).

12 I. Roehle and C. Willert, "Extension of Doppler Global Velocimetry to Periodic Flows", *Measurement Science and Technology*, **12**, 420-431, (2001).

13 R.L. McKenzie, "Measurement capabilities of Planar Doppler Velocimetry using pulsed lasers", *Applied Optics*, **35**, pp 948-964, (1996).

14 G.S. Elliott and T.J. Beutner, "Molecular Filter Based Planar Doppler Velocimetry", *Progress in Aerospace Sciences*, **35**, 799-845, (1999).

15 D.S. Nobes, H.D. Ford, and R.P. Tatam," Planar Doppler Velocimetry Measurements of Flows using Imaging Fiber Bundles", *SPIE proceedings, Optical Diagnostics for Fluids, Solids and Combustion II*, (San Diego, CA, 2003), Vol. 5191, pp 122-133.

16 G.S. Elliott, J. Crafton, T.J. Beutner, C.D. Carter, H.D. Baust, and C. Tyler," Evaluation and Optimization of a Multi-Component Planar Doppler Velocimetry System", *AIAA 43rd Aerospace Sciences Meeting and Exhibit*, (Reno, Nevada, 2005), AIAA 2005-35.

17 D.S. Nobes, H.D. Ford, and R.P. Tatam, "Three Component Planar Doppler Velocimetry Using Imaging Fibre Bundles", *Experiments in Fluids*, **36**, pp 3-10, (2004).

18 T.O.H. Charrett and R.P. Tatam, "Single camera three component planar velocity measurements using two frequency Planar Doppler Velocimetry (2ν-PDV)", *Measurement Science and Technology*, **17**, pp 1194-1206, (2006).

19 I. Roehle, "Three-dimensional Doppler Global Velocimetry in the flow of a fuel spray nozzle and in

the wake region of a car", *Flow Measurement Instrumentation*, **7**, 287-294, (1996).

20 K. Arbenze and A. Wohlhauser, *Advanced Mathematics for Practicing Engineers*, (Artech House, Norwood, MA, USA, 1986).

21 D.S. Nobes, B. Wieneke, and R.P. Tatam, "Determination of View Vectors from Image Warping Mapping Functions", *Optical Engineering*, **43**, 407-414, (2004).

22 E. Kreyszig, *Advanced Engineering Mathematics, 7th Edition*, (Wiley, New York, 1993).

23 T.O.H. Charrett, H.D. Ford, D.S. Nobes, and R.P. Tatam, "Two frequency Planar Doppler Velocimetry (2ν-PDV)", *Review of Scientific Instruments*, **75**, 4487-4496, (2004).

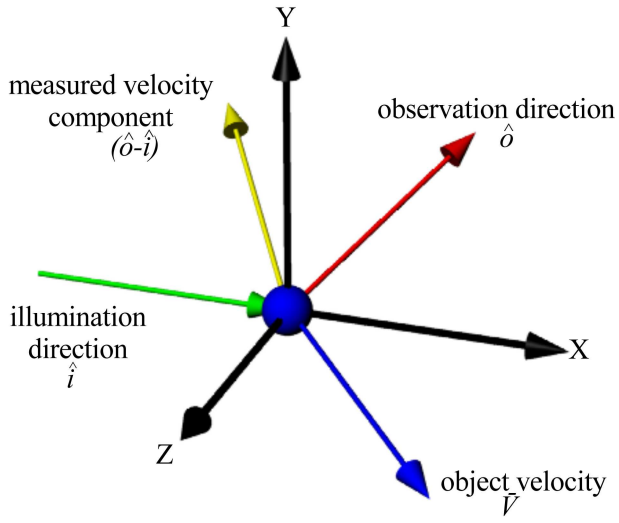

Figure 1. The relationship of laser illumination direction and observation direction to the measured velocity component determined from the Doppler equation. Here $\hat{o}$ is the observation direction, $\hat{i}$ is the laser illumination direction

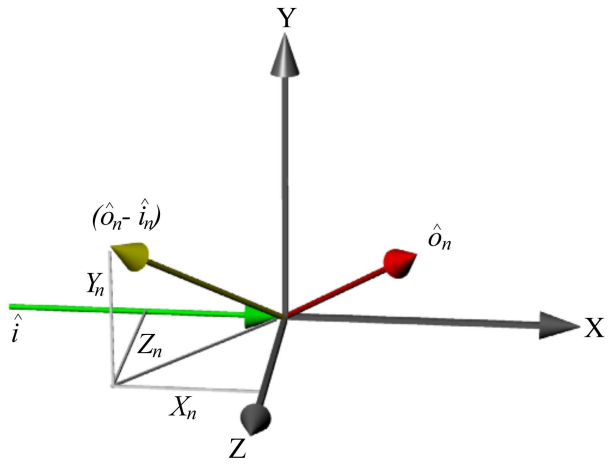

Figure 2. Definitions used in the conversion from measured velocity components to the orthogonal components. Here $\hat{o}_n$ is the observation direction of the nth view and $\hat{i}$ is the laser illumination direction; X_n, Y_n and Z_n are the Cartesian components of the measured velocity $(\hat{o}_n - \hat{i})$ component.

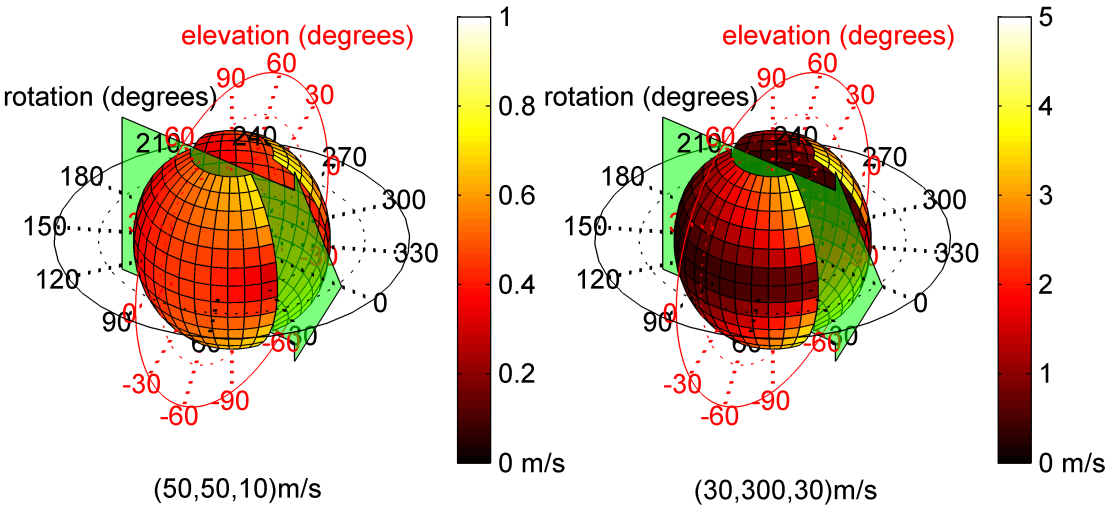

Figure 3. Variation of the uncertainty in the velocity component due to the uncertainty in the angle ϕ (between $\hat{o}$ and $\hat{\imath}$). Positions on the surface represent the observation direction and the colour the magnitude of the velocity uncertainty. The illumination direction is indicated and the uncertainty in the angle ϕ was assumed to be 1^{o}.

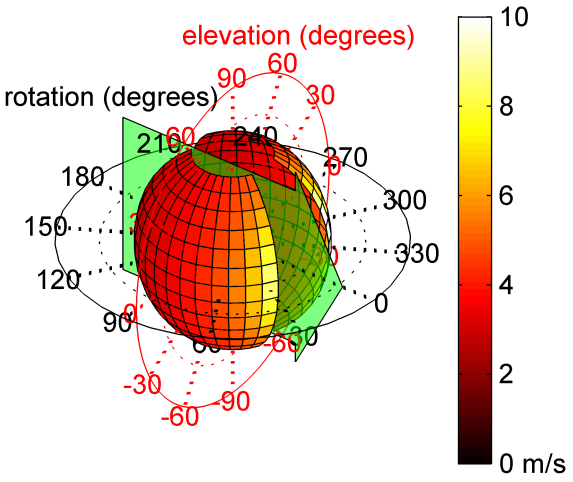

Figure 4. Variation of the uncertainty in the velocity component due to the uncertainty in Doppler shift measurement. The illumination direction is indicated, and the uncertainty in the measurement of Doppler shift was assumed to be 5MHz.

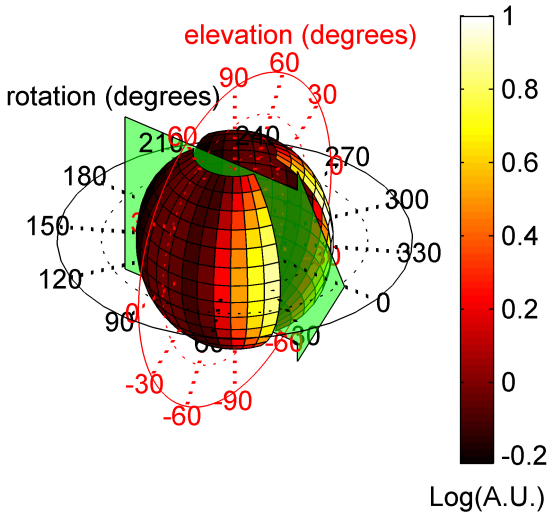

Figure 5. Variation in relative Mie scattering intensity for a seed particles size distribution of 0.1-0.4µm.

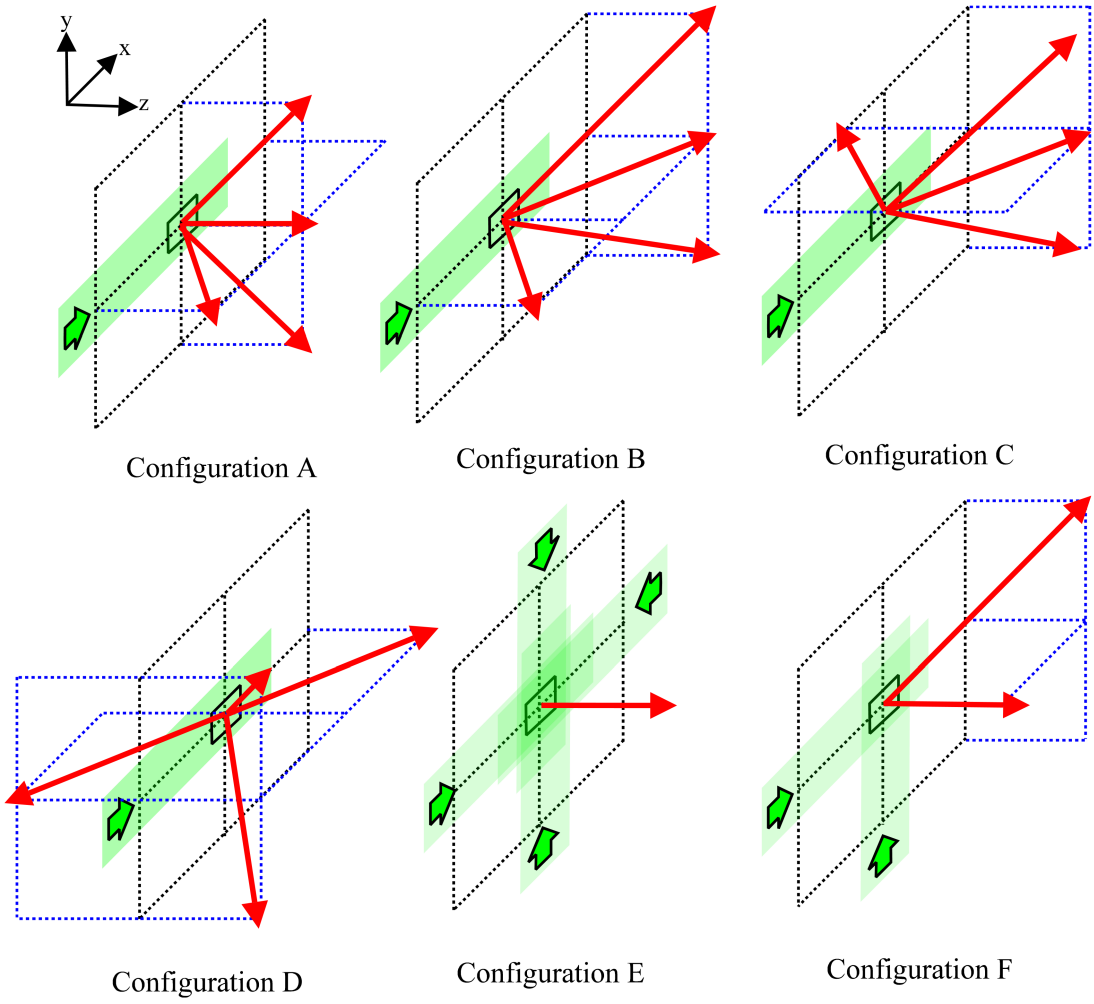

Figure 6. Schematic diagrams showing the viewing configurations used.

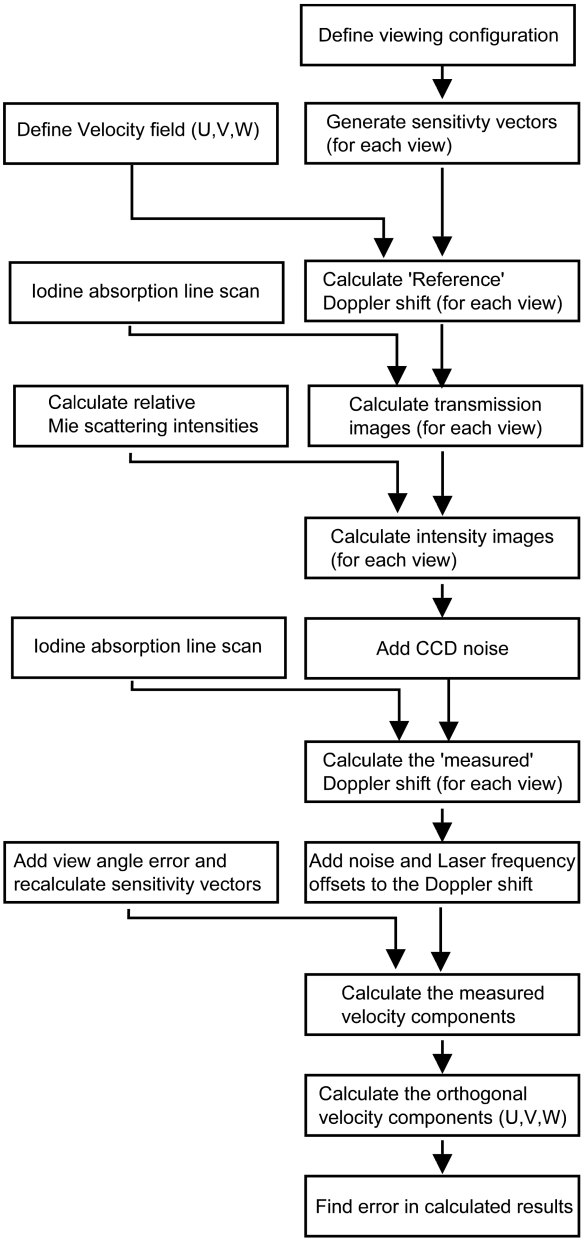

Figure 7. Flow diagram showing the modelling process.

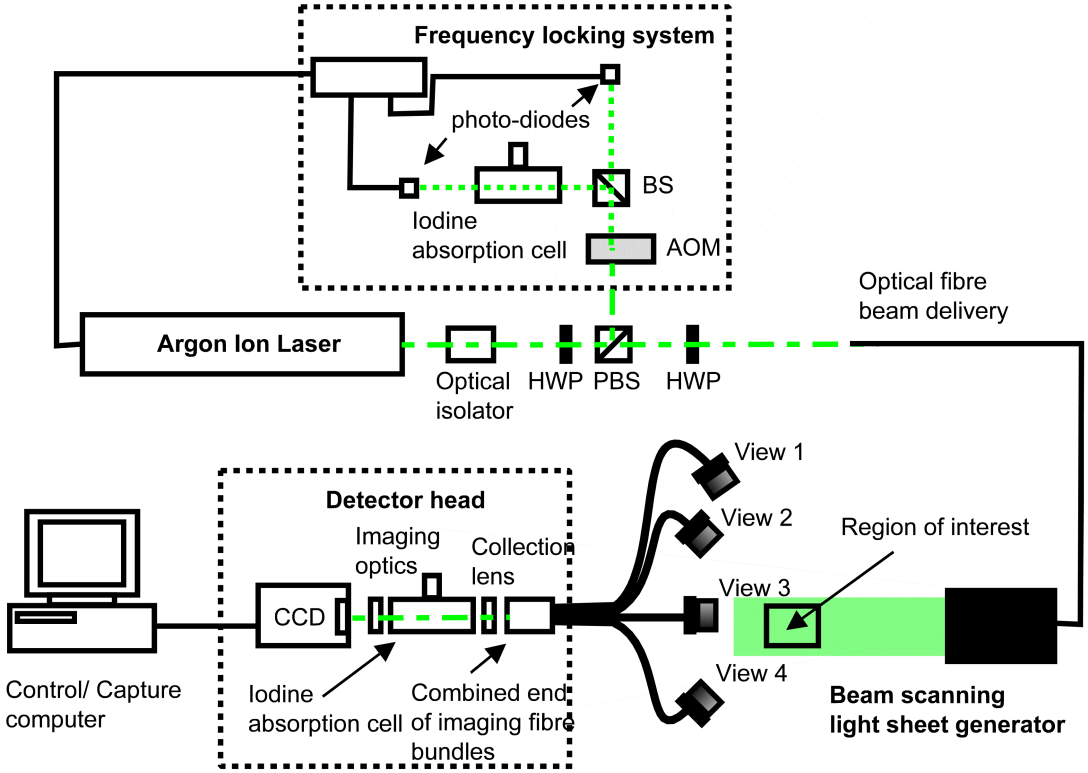

Figure 8. Schematic showing the experimental arrangement used for the three dimensional velocity measurements. AOM – acousto-optic modulator; PBS – polarising beam splitter; BS – beam splitter; HWP – half wave plate.

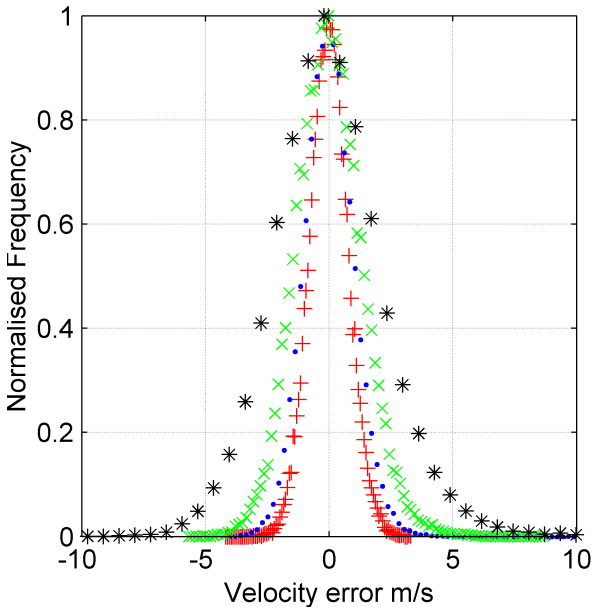

Figure 9. Histograms of the measured error in the velocity components for various values of angle ϕ; 90^o (+), 70^o (•), 50^o (x) and 30^o (*)

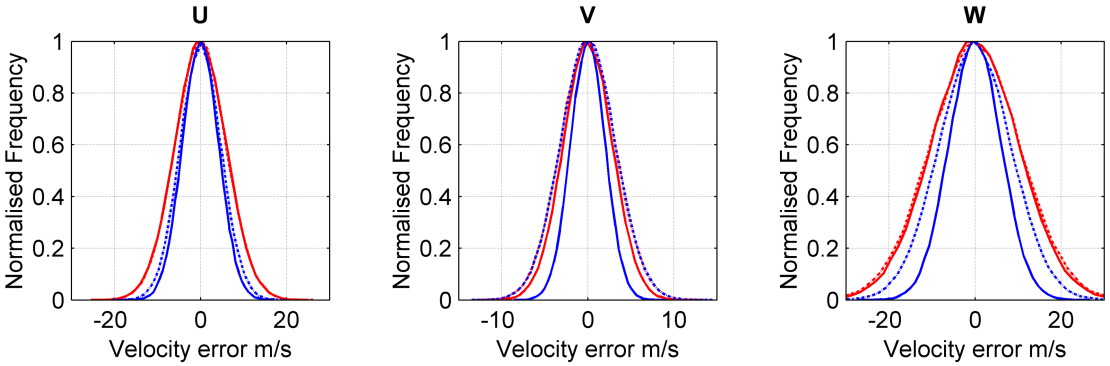

Figure 10. Histograms of the error in the orthogonal components for configuration A (red) and configuration B (blue); Solid lines are for calculation with constant error added to the measured components; Dashed lines (may be obscured) are for calculation with a variation in error due to observation direction. A velocity field of (10,100,10) m/s was used.

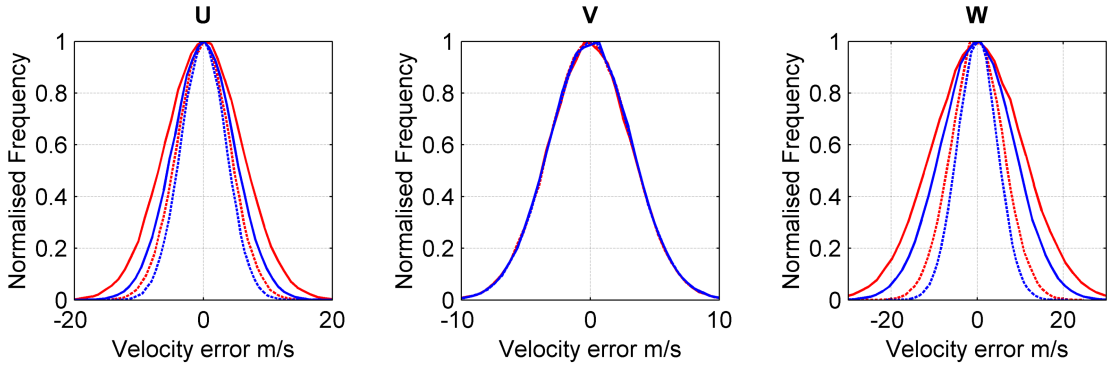

Figure 11. Histograms of error in orthogonal components for configuration A (red) and configuration B (blue). Solid lines show the error using the 3C method of calculating the orthogonal velocity components and the dashed lines show the error using the 4C method.

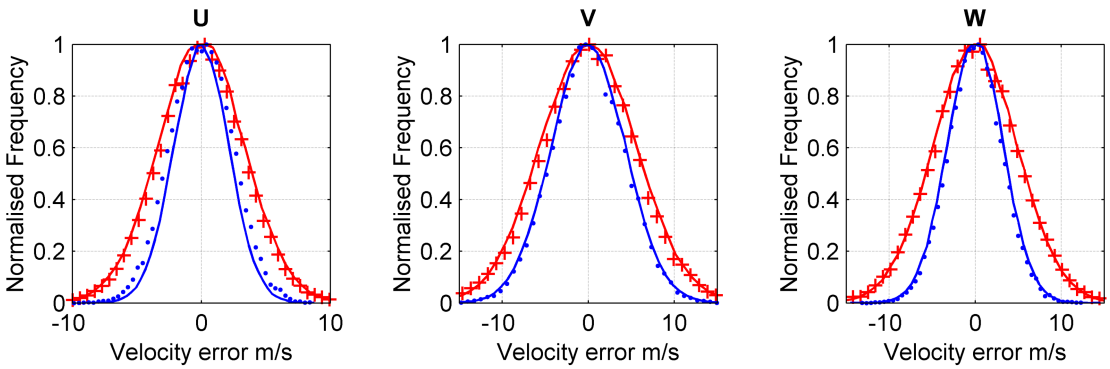

Figure 12. Histograms of the error in the orthogonal components for configuration A (red) and configuration B (blue) for both the simulated (solid line) and experimental results (data points) for the velocity field of a rotating disc.

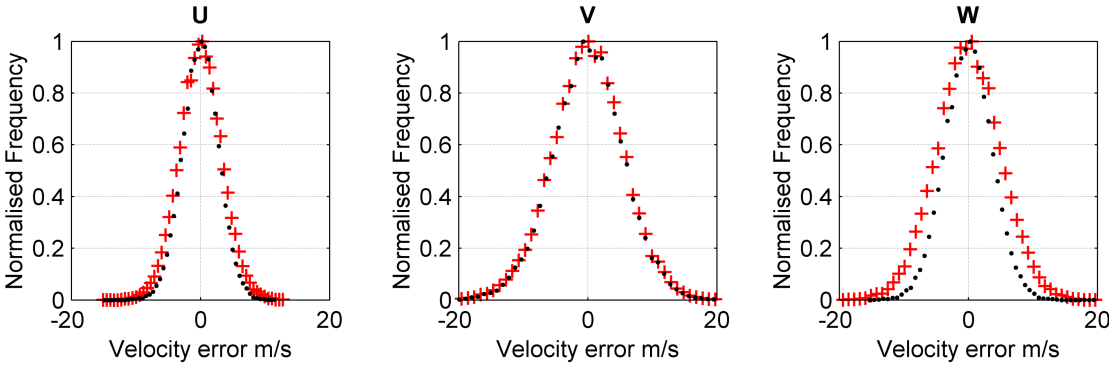

Figure 13. Histograms of the experimental error in the orthogonal components for configuration A using the 3C method (crosses) and the 4C method (dots).

Figure 1. The relationship of laser illumination direction and observation direction to the measured velocity component determined from the Doppler equation. Here $\hat{o}$ is the observation direction, $\hat{\imath}$ is the laser illumination direction

Figure 2. Definitions used in the conversion from measured velocity components to the orthogonal components. Here $\hat{o}_n$ is the observation direction of the nth view and $\hat{\imath}$ is the laser illumination direction; X_n, Y_n and Z_n are the Cartesian components of the measured velocity $(\hat{o}_n - \hat{\imath})$ component.

Figure 3. Variation of the uncertainty in the velocity component due to the uncertainty in the angle ϕ (between $\hat{o}$ and $\hat{\imath}$). Positions on the surface represent the observation direction and the colour the magnitude of the velocity uncertainty. The illumination direction is indicated and the uncertainty in the angle ϕ was assumed to be 1^o.

Figure 4. Variation of the uncertainty in the velocity component due to the uncertainty in Doppler shift measurement. The illumination direction is indicated, and the uncertainty in the measurement of Doppler shift was assumed to be 5MHz.

Figure 5. Variation in relative Mie scattering intensity for a seed particles size distribution of 0.1-0.4μm.

Figure 6. Schematic diagrams showing the viewing configurations used.

Figure 7. Flow diagram showing the modelling process.

Figure 8. Schematic showing the experimental arrangement used for the three dimensional velocity measurements. AOM – acousto-optic modulator; PBS – polarising beam splitter; BS – beam splitter; HWP – half wave plate.

Figure 9. Histograms of the measured error in the velocity components for various values of angle ϕ; 90^o (+), 70^o (•), 50^o (x) and 30^o (*)

Figure 10. Histograms of the error in the orthogonal components for configuration A (red) and configuration B (blue); Solid lines are for calculation with constant error added to the measured components; Dashed lines (may be obscured) are for calculation with a variation in error due to observation direction. A velocity field of (10,100,10) m/s was used.

Figure 11. Histograms of error in orthogonal components for configuration A (red) and configuration B (blue). Solid lines show the error using the 3C method of calculating the orthogonal velocity components and the dashed lines show the error using the 4C method.

Figure 12. Histograms of the error in the orthogonal components for configuration A (red) and configuration B (blue) for both the simulated (solid line) and experimental results (data points) for the velocity field of a rotating disc.

Figure 13. Histograms of the experimental error in the orthogonal components for configuration A using the 3C method (crosses) and the 4C method (dots).

Table 1. Definitions of the viewing configurations used showing the Cartesian components and viewing angles for each observation direction.

Configuration A

	$\hat{o}_1$	$\hat{o}_2$	$\hat{o}_3$	$\hat{o}_4$
X	0.000	0.000	-0.707	0.000
Y	0.707	-0.707	0.000	0.000
Z	0.707	0.707	0.707	1.000
$\alpha(^o)$	90	90	135	90
$\beta(^o)$	45	-45	0	0

Configuration B

	$\hat{o}_1$	$\hat{o}_2$	$\hat{o}_3$	$\hat{o}_4$
X	0.500	0.500	-0.707	0.707
Y	0.707	-0.707	0.000	0.000
Z	0.500	0.500	0.707	0.707
$\alpha(^o)$	45	45	135	45
$\beta(^o)$	45	-45	0	0

Configuration C[8]

	$\hat{o}_1$	$\hat{o}_2$	$\hat{o}_3$	$\hat{o}_4$
X	0.460	0.460	0.383	0.383
Y	0.628	-0.628	0.000	0.000
Z	0.628	0.628	-0.924	0.924
$\alpha(^o)$	54	54	-67	67
$\beta(^o)$	40	-40	0	0

Configuration D

	$\hat{o}_1$	$\hat{o}_2$	$\hat{o}_3$	$\hat{o}_4$
X	-0.500	-0.500	-0.707	0.707
Y	0.707	-0.707	0.000	0.000
Z	0.500	0.500	-0.707	0.707
$\alpha(^o)$	135	135	225	45
$\beta(^o)$	45	-45	0	0

Configuration E[7]

	$\hat{o}_1$	
X	0.000	Four orthogonal laser sheets in the same plane used sequentially (1,0,0), (-1,0,0), (0,1,0) & (0, -1,0)
Y	0.000	
Z	1.000	
$\alpha(^o)$	90	
$\beta(^o)$	0	

Configuration F

	$\hat{o}_1$	$\hat{o}_2$	
X	0.000	0.500	Two light sheets used sequentially (1,0,0) & (0,1,0)
Y	0.000	0.707	
Z	1.000	0.500	
$\alpha(^o)$	90	45	
$\beta(^o)$	0	45	

Table 2. The sensitivity vectors of the ideal case configuration, and the computed matrix conditioning numbers for the different definitions.

	Cartesian components of the measured velocity components / sensitivity vectors		
	X	Y	Z
$(\hat{o}_1 - \hat{i}_1)$	1.000	0.000	0.000
$(\hat{o}_2 - \hat{i}_2)$	0.000	1.000	0.000
$(\hat{o}_3 - \hat{i}_3)$	0.000	0.000	1.000

Condition Numbers			
κ_1	κ_2	κ_3	κ_4
1.000	1.000	3.000	1.000

Table 3. Condition numbers for the viewing configurations used in the investigation (1st three views only)

Configuration	Condition Number			
	κ_1	κ_2	κ_3	κ_4
A	14.75	9.13	10.41	14.55
B	7.11	5.03	6.63	8.98
C	3.47	1.38	3.13	3.23
D	6.15	2.79	4.49	4.68
E	4.50	2.41	3.87	4.00
F	8.45	5.43	7.31	8.95

Table 4. Conditions used in simulation

Parameter	Value
Field of view	100 by 100 mm.
Image size	400 by 400 pixels.
Imaging distance	1.5 m.
Illuminating wavelength	514.5 nm.
Light sheet	Parallel rays with direction $\hat{\imath}$.
Seed particle size range	0.1 –0.4μm*
CCD A/D conversion factor	$5e^-$/count

* Particle size range selected to match the output of the seeder used in previous experimental investigations at Cranfield [17,18,23].

Table 5. Computed standard deviation of orthogonal component residuals (computed values minus original values) for three measured components (3C) with a constant error and variable error on measured velocity components for a velocity field of (10,100,10) m/s

	Condition Number [1]	Standard deviation of computed orthogonal component residuals (m/s)					
		Constant error[2]			Variable error[3]		
		U	V	W	U	V	W
A	14.75	6.0	2.8	10.1	5.9	3.2	10.4
B	7.11	4.2	2.0	6.1	4.8	3.2	8.4
A*	14.75	-	-	-	9.2	7.6	19.8
B*	7.11	-	-	-	7.9	7.1	17.3
C	3.47	2.2	2.3	1.7	3.1	3.4	2.4
D	6.15	1.3	3.5	3.6	1.3	3.3	3.5
E	4.50	2.0	3.5	2.0	2.3	4.3	2.8
F	8.45	6.3	3.5	4.5	7.7	4.8	7.3

(1) Condition number $\kappa 1$;
(2) Constant error, ERR_{Con}, added to components (standard deviation 2.0m/s);
(3) Variable error, ERR_{Var}, added to components - errors calculated using a Doppler shift uncertainty of 2.5 MHz and uncertainty in view angles of 0.1^{o};
* Velocity field of (30,300,30) m/s used.

Table 6. Computed standard deviation of orthogonal component residuals (computed values minus original values) for a velocity field of (10,100,10) m/s.

	Standard deviation of computed orthogonal component residuals (m/s)					
	3C method [1]			4C method [2]		
	U	V	W	U	V	W
A	5.9	3.2	10.4	4.1	3.2	6.0
B	4.8	3.2	8.4	3.5	3.2	4.7
A*	9.2	7.6	19.8	4.4	7.6	6.5
B*	7.9	7.1	17.3	4.0	7.0	5.0
C	3.1	3.4	2.4	2.8	3.5	2.1
D	1.3	3.3	3.5	1.3	3.3	3.2
E	2.3	4.2	2.8	2.0	2.4	1.6
F	7.7	4.8	7.3	4.1	3.6	3.1

[1] 3C method
[2] 4C method with equal weighting of all velocity components.
* Velocity field of (30,300,30) m/s used.

Table 7. Comparison of the computed standard deviation of orthogonal component residuals (computed values minus original values) using the best 3 of 4 views and the 4C method for a velocity field of (10,100,10) m/s. Negative percentage changes indicates a reduction in uncertainty when using the 4C method.

	Standard deviation of computed orthogonal component residuals (m/s)								
	'Best' 3C method			4C method			% Change		
	U	V	W	U	V	W	U	V	W
A	5.2	3.2	7.1	4.1	3.2	6.0	-21.2	0.0	-15.5
B	3.2	3.2	5.1	3.5	3.2	4.7	9.4	0.0	-7.8
A*	4.5	7.6	7.3	4.4	7.6	6.5	-2.2	0.0	-11.0
B*	3.3	7.0	9.6	4.0	7.0	5.0	21.2	0.0	-47.9
C	3.1	3.4	2.3	2.8	3.5	2.1	-9.7	2.9	-8.7
D	1.3	3.3	3.5	1.3	3.3	3.2	0.0	0.0	-8.6
E	2.0	2.4	2.1	2.0	2.4	1.6	0.0	0.0	-23.8
F	4.0	3.7	3.6	4.1	3.6	3.1	2.5	-2.7	-13.9

* Velocity field of (30,300,30) m/s used.

Table 8. Viewing angles used for experimental measurements, (previously defined value)

Configuration	View angle (^{o})	View 1	View 2	View 3	View 4
A	α	180	180	-135	180
	β	21 (45)	-21 (45)	0	0
B	α	135	135	-135	135
	β	21 (45)	-21 (45)	0	0

Table 9. Standard deviation of orthogonal component residuals (experimental values minus theoretical values) for a velocity field of a rotating disc

	Standard deviation of the orthogonal component residuals (m/s)					
	3C method			4C method		
	U	V	W	U	V	W
A	3.25	5.50	4.90	2.81	5.50	3.69
B	2.40	4.22	3.16	2.18	4.22	2.38

Table captions

Table 1. Definitions of the viewing configurations used showing the Cartesian components and viewing angles for each observation direction.

Table 2. The sensitivity vectors of the ideal case configuration, and the computed matrix conditioning numbers for the different definitions.

Table 3. Condition numbers for the viewing configurations used in the investigation (1^{st} three views only)

Table 4. Conditions used in simulation

Table 5. Computed standard deviation of orthogonal component residuals (computed values minus original values) for three measured components (3C) with a constant error and variable error on measured velocity components for a velocity field of (10,100,10) m/s

Table 6. Computed standard deviation of orthogonal component residuals (computed values minus original values) for a velocity field of (10,100,10) m/s.

Table 7. Comparison of the computed standard deviation of orthogonal component residuals (computed values minus original values) using the best 3 of 4 views and the 4C method for a velocity field of (10,100,10) m/s. Negative percentage changes indicates a reduction in uncertainty when using the 4C method.

Table 8. Viewing angles used for experimental measurements, (previously defined value)

Table 9. Standard deviation of orthogonal component residuals (experimental values minus theoretical values) for a velocity field of a rotating disc